

Residual Temperature Bias Effects in Stratospheric Species Distributions from LIMS

Ellis Remsberg¹, V. Lynn Harvey², Arlin Krueger³, and Murali Natarajan¹

¹Science Directorate, NASA Langley Research Center, 21 Langley Blvd, Mail Stop 401B,
Hampton, VA 23681, USA

²Laboratory for Atmospheric and Space Physics, University of Colorado Boulder, 3665
Discovery Drive, Boulder, CO 80303, Colorado, USA

³Emeritus Senior Scientist, Code 614 Atmospheric Chemistry and Dynamics Laboratory, NASA
Goddard Space Flight Center, Greenbelt, MD 20771, USA

Correspondence to: Ellis Remsberg (ellis.e.remsberg@nasa.gov)

(For submission to Atmospheric Measurement Techniques Journal)

~~December, 2020~~

January, 2021

Abstract

The Nimbus 7 Limb Infrared Monitor of the Stratosphere (LIMS) instrument operated from October 25, 1978, through May 28, 1979. Its Version (V6) profiles were processed and archived in 2002. We present several diagnostic examples of the quality of the V6 stratospheric species distributions based on their Level 3 zonal Fourier coefficient products. In particular, we show that there are small differences in the ascending (A) minus descending (D) orbital temperature-pressure or T(p) profiles (their A-D values) that affect (A-D) species values. Systematic A-D biases in T(p) can arise from small radiance biases and/or from viewing anomalies along orbits. There can also be (A-D) differences in T(p) due to not resolving and correcting for all of the atmospheric temperature gradient along LIMS tangent view-paths. An error in T(p) affects species retrievals through: (1) the Planck blackbody function in forward calculations of limb radiance that are part of the iterative retrieval algorithm of LIMS, and (2) the registration of the measured LIMS species radiance profiles in pressure-altitude, mainly for the lower stratosphere. There are clear A-D differences for ozone, H₂O, and HNO₃, but not for NO₂. Percentage differences are larger in the lower stratosphere for ozone and H₂O because those species are optically thick. We evaluate V6 ozone profile biases in the upper stratosphere with the aid of comparisons against a monthly climatology of UV-ozone soundings from rocketsondes. We also provide results of time series analyses of V6 ozone, H₂O, and potential vorticity for the middle stratosphere to show that their average (A+D) V6 Level 3 products provide a clear picture of the evolution of those tracers during northern hemisphere winter. We recommend that researchers use the average V6 Level 3 product for their science studies of stratospheric ozone and H₂O, but keeping in mind that there are uncorrected NLTE effects in daytime ozone in the lower mesosphere and in daytime H₂O in the uppermost stratosphere. We also point out that the present-day Sounding of the Atmosphere using Broadband Emission Radiometry (SABER) experiment provides measurements and retrievals of temperature and ozone that are more nearly free of anomalous diurnal variations [and of effects from gradients](#) at low and middle latitudes.

1 Introduction and objectives

The historic Nimbus 7 Limb Infrared Monitor of the Stratosphere (LIMS) experiment provided data on the middle atmosphere from October 25, 1978, through May 28, 1979, for scientific analysis and for comparisons with atmospheric models (Gille and Russell, 1984). Remsberg et al. (2007) describe characteristics of the ozone profiles of the LIMS Version 6 (V6) dataset. Notably, V6 corrects for a high ozone bias in the lowermost stratosphere of the previous Version 5 (V5) profiles, as shown by comparisons of the V6 profiles with ozonesonde data in Remsberg et al. (2007; 2013). Remsberg et al. (2009) report on improvements in the profiles and distributions of V6 water vapor (H_2O) within the lower stratosphere, where temperature and interfering radiances from the oxygen continuum are more accurate than in the processing of V5. Finally, Remsberg et al. (2010) contain information on the V6 improvements of nitric acid (HNO_3) and, in particular, nitrogen dioxide (NO_2).

Frith et al. (2020) reported on modeled estimates of diurnal ozone variations, as a function of latitude, altitude, and season. In general, their modeled results are in accord with observed ozone variations from both satellite ultraviolet (uv) and microwave measurements. However, the ozone distributions from the infrared measurements of LIMS show some anomalously large day/night differences in the middle stratosphere (Remsberg et al., 1984; 2007). LIMS ozone and H_2O are quite sensitive to small biases of the LIMS temperature versus pressure, or $T(p)$, due to nonlinear effects of the Planck blackbody function in forward radiance calculations that are part of the LIMS retrieval algorithm (Gille et al., 1984; Remsberg et al., 2004). Consequently, temperature bias is the largest source of ozone and H_2O error, by far, although ~~such small~~ bias effects from $T(p)$ are hard to verify from correlative comparisons of individual profiles. The LIMS orbital line-of-sight to its tangent layer is nearly in a meridional direction or along horizontal temperature gradients (Gille and Remsberg et al., 1984; 1990). Roewe et al. (1982) ~~showed that it is important to incorporate~~ consider line-of-sight ~~$T(p)$~~ radiance gradient corrections for the LIMS species retrievals. ~~While, while~~ Gille et al. (1984) employ corrections based on the $T(p)$ gradient. ~~We will show that while~~ the LIMS algorithm makes first-order corrections for $T(p)$ gradients, residual bias effects are still apparent in the V6 species distributions.

This study considers the distributions of V6 T(p) plus plots of ascending (A) minus descending (D) orbital differences (A-D) for both temperature and species, as diagnostics for the effects of residual bias errors in T(p). We evaluate those effects using plots of the LIMS ~~V6~~-Level 3 (mapped) products (Remsberg et al., 1990; Remsberg and Lingenfelter, 2010) and their monthly zonal mean distributions that are part of the SPARC Data Initiative (SPARC, 2017). Section 2 gives a brief review of the characteristics and retrieval algorithms for V6 temperature and species. Section 3 reviews the measurement, retrieval, and day/night differences for temperature. Section 4 relates small temperature biases to the anomalous A-D values in the LIMS monthly species distributions for March 1979. Section 5 compares V6 daytime ozone with rocketsonde UV-filter ozone (ROCOZ) profile data for the upper stratosphere and lower mesosphere. We interpret the comparisons according to their respective error estimates and by examining the profiles in the context of hemispheric maps of the surrounding temperature and ozone fields from the Level 3 products. Section 6 contains results of time series of northern hemisphere (NH) distributions of V6 ozone and H₂O on the 850 K potential temperature surface (~10 hPa), as indications of the quality of averages of their V6 data. Section 7 summarizes our findings about the V6 species and our recommendations for scientific studies of them. We also point out why the follow-on experiment, Sounding of the Atmosphere using Broadband Emission Radiometry (SABER), provides measurements and retrievals of temperature that are nearly free of anomalous A-D differences at low and middle latitudes.

2 Characteristics of the V6 Level 3 ozone, temperature, and water vapor

2.1 Daily mapped data

The V6 algorithm accounts for low-frequency spacecraft motions that affect how the LIMS instrument views the horizon and the subsequent registration of its measured radiance profiles in pressure-altitude (Remsberg et al., 2004). Retrieved ozone, temperature, and geopotential height (GPH) profiles extend from 316 hPa to ~0.01 hPa and have a point spacing of ~0.88 km with a vertical resolution of ~3.7 km. H₂O, HNO₃, and NO₂ data are limited to the stratosphere (~100 hPa to 1 hPa). Processing of the original V5 T(p) profiles occurred at a rather coarse vertical point spacing of ~1.5 km and for every ~4 degrees of latitude. Retrievals for V6 occur at every ~1.6 degrees of latitude along orbits and resolve the horizontal temperature structure better.

108 However, the ~~horizontal~~ line-of-sight $T(p)$ gradients for both the V5 and V6 processing
109 algorithms are from daily maps of the combined V5 (A+D) temperature fields on pressure
110 surfaces.

111
112 Mapping of the V6 profiles to a Level 3 product occurs at 28 vertical levels, as opposed to just
113 18 levels for V5. The sequential-estimation mapping algorithm for V6 (Remsberg and
114 Lingenfelter, 2010) employs a shorter relaxation time of about 2.5 days for its zonal wave
115 coefficients, compared with ~5 days for V5. The mapping algorithm is insensitive to the very
116 few large, unscreened ozone mixing ratio values within the lower stratosphere, as noted in
117 Remsberg et al. (2013, Fig. 1a). LIMS made measurements with a duty cycle of up to 11 days
118 on and 1 day off, and the mapping algorithm interpolates the profile data in time to provide a
119 continuous, 216-day set of daily zonal coefficients. Daily maps also provide a spatial context for
120 the individual V6 profiles and are helpful for interpreting comparisons with auxiliary data sets,
121 especially during dynamically disturbed periods.

122 123 *2.2 Monthly zonal average V6 ozone, temperature, and water vapor*

124 We generated monthly zonal mean distributions from the daily Level 3 files of temperature and
125 species and supplied them to the SPARC Data Initiative or SPARC-DI (SPARC, 2017).
126 Although the V6 ozone for SPARC-DI extends up to only the 0.1-hPa level (~64 km), Figure 1
127 updates the combined (A+D), monthly ozone for March 1979 to its highest level of about 0.015
128 hPa (~75 km). Retrieved daytime ozone contributes to the (A+D) ozone in Fig. 1 and has a large
129 positive bias throughout the mesosphere because the LIMS algorithms do not account for non-
130 local thermodynamic equilibrium (NLTE) effects from either ozone (Solomon et al., 1986;
131 Mlynczak and Drayson, 1990) or CO_2 (Edwards et al., 1996; Manuilova et al., 1998). However,
132 the V6 nighttime ozone is essentially free of those NLTE effects below about the 0.05-hPa level.
133 We also screened the SPARC-DI product of daily zonal mean ozone values (<0.1 ppmv) near the
134 tropical tropopause, as recommended in Remsberg et al. (2013). This study focuses on the
135 quality of V6 ozone in the stratosphere.

Figure 1 shows that ozone has largest mixing ratios at about 10 hPa near the Equator (~10.8 ppmv), decreasing sharply above and below that level. Maximum mixing ratios at the middle to high latitudes occur closer to 3 hPa, due to larger zenith angles and longer paths of the uv light for the production of its atmospheric ozone. Remsberg et al. (2007) compared V6 ozone and Solar Backscatter UltraViolet (SBUV) Version 8.0 ozone and reported that V6 ozone is larger (by 4 to 12%) in the upper stratosphere, although the differences are within the combined errors of V6 and SBUV. However, the monthly comparisons at 4 hPa indicate that those differences increase from November to May. Sun and Leovy (1990, their Fig. 1) also compared Equatorial ozone time series from LIMS and SBUV, and they found that their monthly differences for the upper stratosphere changed with the descent of the semi-annual oscillation (SAO). Most likely, LIMS and SBUV do not resolve the vertical response of ozone to the SAO equally well.

Figure 2 shows the March zonal mean V6 T(p) distribution from SPARC-DI. Monthly T(p) extends to near the 0.01-hPa level and has values every 5° of latitude. T(p) has a maximum value of about 275 K at the stratopause and minimum values approaching 195 K near the mesopause and at the tropical tropopause. Radiances from the two 15-μm CO₂ channels for retrievals of T(p) are free of NLTE effects below about the 0.05-hPa level (~70 km) (Lopez-Puertas and Taylor, 2001). Estimates of a bias in V6 T(p) are in Table 1 (row 2), according to Remsberg et al. (2004, their Table 2, row g-) but not including any error due to temperature gradients. Estimates of bias errors for ozone due to those T(p) errors are in Table 1 (row 3); a positive bias in temperature leads to a negative bias in retrieved ozone (and ~~in H₂O~~ the other species) via the effect of the Planck function on radiance calculations. In principle, one may also infer the quality of the V6 temperatures based on independent estimates of the quality of the retrieved ozone. Table 1 (last row) compares V6 T(p) for March 1979 at 38°N with that from the temperature climatology at 40°N from Barnett and Corney (or BC, 1985). Those (V6 – BC) temperature values include a five-point running average of the SPARC-DI V6 monthly T(p) profile above the 30-hPa level to account for the broader vertical weighting functions of the satellite measurements of BC. The difference profiles, V6-BC, have values of the order of the bias estimates for V6 T(p) (in row 2). The larger difference of -4.4 K at 3 hPa indicates the

redistribution of northern hemisphere temperature following the final stratospheric warming and split vortex that is specific to late February 1979.

Figure 3 shows V6 zonal average H₂O for March 1979 from SPARC-DI. Highest values of H₂O are at upper altitudes (> 6.0 ppmv) and are due to the oxidation of methane (CH₄) to H₂O, followed by its net transport and accumulation at higher latitudes. H₂O is effectively a tracer of the mean meridional circulation, which moves upward from the tropical tropopause to the middle stratosphere and then poleward toward higher latitudes. Minimum zonal-mean values of H₂O are of order 3.5 ppmv in the tropics between 50 and 70 hPa. The sharply increasing H₂O near the tropical tropopause may be due, in part, to residual radiance from cirrus cloud tops. The V6 species have a first order screening for clouds at latitudes between $\pm 30^\circ$ and for pressure-altitudes below 45 hPa, according to a threshold criterion of the vertical slope of the co-located ozone mixing ratio profiles (see Sections 2.2 in Remsberg et al., 2007; 2009). Locations of cloud tops are in separate daily files that are a part of the V6 Level 2 or daily profile data set. NLTE processes also cause enhancements of H₂O radiance near the stratopause during daytime. Those uncorrected NLTE effects extend downward to lower altitudes for retrieved V6 H₂O, although the effects are small for the middle and lower stratosphere (Mertens et al., 2002). Estimates of the effect of temperature bias for V6 H₂O are in Table 1 (row 4) from Remsberg et al. (2009).

3 Measurement, retrieval, and day/night differences for temperature

Nimbus 7 was in a near-polar orbit, and LIMS made measurements at ~1 pm local time along its ascending (A or south-to-north traveling) orbital segments and at ~11 pm for its descending (D or north-to-south traveling) segments. The A-D time difference is of the order of 10 hours because LIMS viewed the atmosphere 146.5° clockwise of the spacecraft velocity vector or 33.5° counterclockwise from its negative velocity vector, as seen from overhead. In other words, LIMS viewed atmospheric tangent layers in opposing meridional directions for the NH and through the tropics or toward the SSE along A segments and toward the NNW along D segments (Gille and Russell et al., 1984; Remsberg et al., 1990). The A and D view paths for middle

latitudes of the SH are more nearly in a zonal direction and toward the NNW, respectively, due to the orbital inclination of Nimbus 7.

Figure 4 shows V6 A-D temperatures for March. The differences of the upper stratosphere indicate how well the effects of the temperature tides have been resolved (Remsberg et al., 2004). Tropical differences are due mainly to diurnal tides, and they become large in the mesosphere. Tidal amplitudes for the tropics increase with altitude in Fig. 4, ranging from -2 K at 15 hPa to +4 K at 1.5 hPa. Those V6 tidal variations agree qualitatively with ones from rocket Datasonde profiles (Hitchman and Leovy, 1985; Finger et al., 1975). Fig. 4 also shows the expected 180° change of tidal phase for A-D T(p) from the tropics to subtropics. Accurate determinations of T(p) versus latitude depend critically on knowledge of the Nimbus 7 spacecraft attitude. That information for a complete orbit comes empirically from profiles of calculated-to-measured radiance ratios for the LIMS narrow CO₂ channel and can lead to a bias error for A-D T(p). Although orbital attitude bias will affect T(p) at all altitudes, that error source is small according to the good comparisons of the LIMS-derived geopotential heights versus those from operational analyses at both the 10-hPa and 46-hPa levels (Remsberg et al., 2004). Even so, Fig. 4 also shows that there are residual A-D T(p) differences at 70 hPa that are opposite in sign at 40°S and 30°N, or just where there are large, opposing meridional gradients in T(p) in Fig. 2.

Measured ozone radiance profiles contain the full effects of any atmospheric variations in T(p). As an example, Figure 5 shows zonal mean, ozone radiance differences (A-D) for one day (March 15). Radiance differences in the tropics have a change in sign from positive at 3 hPa to negative in the lower mesosphere, and they correspond directly with the A-D changes of temperature in Fig. 4. Positive A-D radiances at middle latitudes of the lower mesosphere are due to the dominance of NLTE daytime radiances from CO₂ and O₃, as compared with the tidal effects from T(p).

There are negative A-D ozone radiances of up to -5% at the northern middle latitudes of the stratosphere, and they are a result of the meridional decrease of T(p) (in Fig. 2) from the northern

subtropics toward higher latitudes. More of the measured radiance in that region comes from the front end of the tangent layer or from the colder side on the A orbital segment and from the warmer side on the D segment, leading to negative A-D radiances. Gille et al. (1984) found that the corresponding A-D temperature differences extend to 4 K or even greater at high northern latitudes. The LIMS algorithms for temperature and species account for horizontal temperature gradients on a pressure surface, ~~but then~~ in the following manner. Daily, near-global temperature fields were obtained from a mapping of the T(p) profiles from a V5 first-pass retrieval. The mapped fields are at 18 separate pressure levels (spaced vertically by 2.3 to 4.3 km, depending on level). Temperature gradients for each profile were determined from the maps, according to the LIMS tangent-path viewing direction in longitude and latitude, and new, second-pass T(p) retrievals were performed taking account of those gradients. V5 gradient estimates from the similar V5 Level 3 map product were used for the processing of the V6 profiles. The T(p) gradient values for each profile are on the archived V6 Level 2 files and used for retrievals of the species. While both the V5 and V6 temperature profile biases become smaller after gradient correction, one must remember that our analyzed temperature gradient information is approximate.

The A-D T(p) differences may still be of order 1 to 2 K after correction (~~Roewe et al., 1982; see Figs. 4 and 5 in~~ Gille et al., 1984; Remsberg et al., 2004 and 2007). Kiefer et al. (2010) analyzed for the effects of a T(p) gradient in more detail using data from the limb-infrared, Michelson Interferometer for Passive Atmospheric Sounding (MIPAS) experiment. They confirm the need to correct for T(p) gradients in the respective A and D views for accurate retrievals of species from the MIPAS A and D radiance profiles. We emphasize that the T(p) gradients for LIMS V6 are from daily surface maps of average (A+D) V5 temperature fields, where the meridional resolution of the V5 fields is no better than half that of V6, or 4° versus 2° of latitude. Those V5 average (A+D) T(p) gradients underestimate the true atmospheric gradients and can result in slight biases between the A and D T(p) values for V6 at the same given latitude.

V6 retrievals of T(p) employ a starting reference pressure level P_0 near 20 hPa (~26 km relative altitude) plus hydrostatic conversions to pressure-altitude that extend both upward and

253 downward from P_0 . The algorithm makes forward radiance calculations for the two broadband
254 CO_2 channels and compares them with their measured radiance profiles. $T(p)$ (A-D) differences
255 of the same sign will impart growing A-D radiance versus pressure differences away from P_0 .
256 Both P_0 and $T(p)$ undergo iteration until the calculated and measured, tangent layer radiances
257 agree to within the noise levels of the measured radiances over the pressure range of 2 to 20 hPa.
258 Yet, the noise value is nearly 2% of the signal at 2 hPa for the narrow CO_2 channel. This
259 pressure level is where the diurnal temperature tide has a larger amplitude and can impart a
260 systematic, A-D bias in P_0 . A-D bias errors in radiance versus pressure are also significant; a
261 radiance calibration error of 1% causes a 0.6 K error in $T(p)$ for the middle and upper
262 stratosphere (Remsberg et al., 2004, Table 3). Another possible source of (A-D) bias for $T(p)$
263 can arise from a residual uncertainty of the viewing attitude of LIMS along an orbit, its empirical
264 “twist factor”.

265
266 Roewe et al. (1982) showed that adjustments for horizontal gradients in $T(p)$ affect species
267 retrievals through calculations of the Planck blackbody radiance, as well as from the registration
268 of their radiance versus pressure profiles, mainly in the lower stratosphere. The region of
269 negative, A-D ozone channel radiance in Fig. 5 has values that increase toward the lower
270 stratosphere because of persistent A-D $T(p)$ biases plus the hydrostatic registration of the
271 measured radiance profiles with pressure-altitude. The radiance differences are negative at
272 middle latitudes of the NH but positive in the SH. Ozone radiance at 10 hPa (not shown)
273 increases from 40°N to 18°N, holds nearly steady in the tropics, and decreases from 20°S to
274 40°S, mainly due to the changing ozone with latitude (Fig. 1). Gordley and Russell (1981)
275 showed that the bulk of the LIMS broadband ozone radiance for the middle and lower
276 stratosphere comes from the near side of the tangent layer (displaced toward the satellite by
277 about 300 to 500 km or $\sim 3^\circ$ to 6° of latitude). That tangent layer weighting explains part of the
278 observed change of sign of the A-D radiances between the two hemispheres in Fig. 5.
279 Nevertheless, the mass path algorithm of the V6 forward model simulates radiance along a well-
280 resolved limb path, using rigorous ray tracing methods, including refraction effects and the first-
281 order corrections for temperature gradients, and assigns an observed tangent altitude
282 corresponding to the center of the measurement field-of-view.

283

284 Roewe et al. (1982) also showed that adjustments for the path gradients of the ozone mixing ratio
285 itself imparts only small A-D mixing ratio differences (~2%). Thus, V6 retrievals do not account
286 for species gradients. The V6 algorithms are no longer operational for further detailed studies of
287 the effects of T(p) gradients for the LIMS species. Instead, in the next section we present
288 diagnostic plots based on the V6 Level 3 data themselves to indicate that there are residual biases
289 in the distributions of V6 T(p) and that they carry over to the V6 species.

290

291 **4 Day/night differences in V6 species**

292 *4.1 Upper stratospheric ozone and H₂O*

293 Remsberg et al. (1984; 2007) reported on the occurrence of day/night, or the A-D ozone values;
294 those results are similar for V5 and V6. Figure 6 shows the distribution of V6 A-D ozone for
295 March as divided by the zonal mean ozone, such that the pattern of systematic differences is a
296 percentage of the zonal average ozone. Photochemical calculations by Haigh and Pyle (1982)
297 predict about a -2% change in ozone for a +1 K change in T(p) at 1.5 hPa. The V6 tropical
298 ozone differences in Fig. 6 grow to nearly -3% near 1 hPa and are opposite in sign to the
299 temperature tides of Fig. 4. Thus, the V6 ozone of the tropical upper stratosphere agrees
300 reasonably with effects from the observed temperature tides.

301

302 Sakazaki et al. (2013, their Fig. 4) also reported diurnal model calculations of tropical day-night
303 ozone values of -3.5% at 44 km (~1.7 hPa) at the local times of the LIMS observations; their
304 microwave observations of ozone agree with them. They also obtained A-D ozone variations of
305 +3.5% at 34 km (~6 hPa) from the photochemistry of odd oxygen during daytime, and those
306 differences decay away from the Equator. Yet, the V6 A-D tropical ozone differences of Fig. 6
307 are nearly twice as large at 6 hPa, and they disagree with modeled changes in Frith et al. (2020).
308 There are also separate, rather large V6 ozone differences at middle latitudes of the upper
309 stratosphere, where effects from temperature tides are small. The rather large A-D ozone values
310 (~4 to 6%) at SH middle latitudes correspond to where the A-D ozone radiances in Fig. 5 are

311 increasing with altitude by +2 to +4% and where A-D $T(p)$ is weakly negative. While these
312 results are consistent with the effects of temperature on retrieved ozone through the V6
313 algorithm, the ozone radiances may also have an A-D pressure registration bias due to the
314 persistently, negative A-D $T(p)$ in that region. The axis of the positive A-D ozone anomaly at
315 NH middle latitudes in Fig. 6 overlays the region of rather large, meridional $T(p)$ gradients in
316 Fig. 2.

317
318 Figures 7 and 8 provide supporting evidence that uncorrected, residual temperature gradients are
319 a likely cause of the A-D ozone anomalies in Fig. 6. Fig. 7 shows zonal (wave) standard
320 deviations (SD) about the zonal average of the combined (A+D) temperature fields for March,
321 where the SD values are from the LIMS SPARC-DI data product. There is significant zonal
322 wave activity at middle to high latitudes in both the NH and SH, and one must account for their
323 separate A and D horizontal gradients for accurate ozone retrievals. Fig. 8 is the corresponding,
324 zonal wave standard deviations for ozone that have a maximum value of 0.40 ppmv near 65°N
325 and 1 hPa, or where transport affects the ozone as well as chemistry.

326
327 V6 H_2O retrievals are more sensitive than ozone to biases in $T(p)$ at 3 hPa (in Table 1) because
328 most of the V6 H_2O radiance comes from its strong, nearly saturated lines. Figure 9 shows H_2O
329 A-D mixing ratio values for March. Both species are altered by horizontal gradients in $T(p)$ in
330 the same way in calculations of their Planck radiances. The locus of maximum percentage
331 difference for H_2O in the SH middle to upper stratosphere differs from that for ozone (Fig. 6)
332 because their respective mixing ratios also have gradients that differ. The effect of the tropical
333 temperature tide on H_2O is not apparent at 1.5 hPa because of the excess of NLTE radiance for
334 V6 daytime H_2O at and above that level.

335

336 *4.2 Middle and lower stratosphere ozone and H_2O*

337 V6 A-D ozone mixing ratio in Fig. 6 is near zero at 20 hPa. This feature occurs where V6 A-D
338 for $T(p)$ in Fig. 4 is also small, or where there is iteration of P_0 and a hydrostatic integration both

above and below that level. The ozone differences become negative below that level across the tropics and in the NH, where the vertical gradient of ozone (Fig. 2) is large and subject to small A-D differences for the registration of the ozone radiance profiles. However, the ozone differences at SH middle latitudes remain positive down to the 100-hPa level; only tangent views along the descending orbital path are in a nearly meridional direction at those latitudes. In particular, the A-D ozone values in Fig. 6 are rather large at 40°S and at 30°N (40 to 100 hPa), and they are opposite in sign to the A-D T(p) differences of order ± 1 K in Fig. 4. This finding agrees with the estimates of T(p) effects at 50 hPa in Table 1, where a bias of -1.3 K leads to a +20% bias in ozone. The A-D temperature biases are large just where the meridional temperature gradients are also large (Fig. 2) and where corrections for them ~~may be~~ too small.

A-D values for H₂O in Fig. 9 have an opposite character from those of ozone from 50 to 100 hPa because the vertical gradient of H₂O in Fig. 3 is also opposite that of ozone in the lowermost stratosphere. This finding is a clear indication of how the same A-D T(p) biases can affect retrieved ozone and H₂O differently. The few correlative balloon measurements of H₂O during 1978/1979 are too uncertain to judge whether the V6 H₂O A or D profiles are more accurate.

One particular feature is that both A-D ozone and H₂O are positive and approach 8% at about 10 hPa and 25°N. The SD values for temperature and ozone show local increases there, too. Fig. 10 gives details of the NH distribution of V6 ozone on the 10-hPa surface for one day, March 15, from a gridding (at 2° lat; 5.625° long) of its 13 zonal Fourier coefficients (a zonal mean and 6 cosine and sine values) in the Level 3 product (Remsberg and Lingenfelser, 2010). There is a meridional ozone gradient at the equatorward edge (~25°N) of a much larger mid latitude region of near zero gradient—a result of effects of an efficient mixing with air from higher latitudes during late winter. Zonal average, A-D temperatures at 10 hPa in Fig. 4 are of order -1 K at 15°N but then change to weakly positive at 25°N. The corresponding NH field of T(p) on March 15 is in Fig. 11, and it shows a narrow belt of slightly higher temperature near 25°N, or just where the A-D meridional T(p) gradient has a change sign in Fig. 4. Such small T(p) differences also affect the registration of the ozone and H₂O radiance profiles. There are unexpected, tropical A-D ozone mixing ratios of order 5% at 10 hPa for all the LIMS months. Those

anomalies appear to migrate seasonally across the tropics and subtropics (see temperature and ozone results for other selected months in the *Supplemental Material*).

4.3 Stratospheric HNO_3 and NO_2

LIMS HNO_3 is optically thin and its retrievals are much less sensitive to temperature bias via the Blackbody function (Table 1, row 5). Its radiance profile measurements also come more nearly from the center of the tangent layer, unlike those of ozone and water vapor. Maximum mixing ratios for HNO_3 occur at about 20 hPa in the tropics and 30 hPa at high latitudes (e.g., as in Fig. 1 of Remsberg et al., 2010) or similar to those of ozone. Figure 12 is a plot of A-D for V6 HNO_3 (in %) for March for comparison with that of ozone in Fig. 6, and there are two important differences between them. First, A-D for HNO_3 in the middle and upper stratosphere is uniformly negative due to its photolysis during daytime, whereas A-D for ozone is slightly positive from enhanced production during the day. Secondly, there are no apparent variations in A-D for HNO_3 in the upper stratosphere at 40°S and near 10 hPa at 25°N from the effects of co-located, horizontal temperature gradients. Yet, the patterns with latitude of A-D in the lower stratosphere are very similar for both HNO_3 and ozone and indicate the effects of A-D temperatures on the registration of the radiance profiles, prior to their retrieval to mixing ratios.

LIMS measured NO_2 radiances at around 1300 and 2300 hours from the Equator to 60°N but changed quickly to 1445 and 2118 hours by 80°N. There is a more gradual change in viewing times for the southern hemisphere from 1323 to 2237 hours at 20°S and then from 1545 and 2015 hours at 60°S, all due to the orbital viewing geometry of LIMS (Gille and Russell, 1984). V6 NO_2 mixing ratios decrease rapidly after sunrise and then increase sharply again at sunset. There is also a slow conversion of NO_2 to NO_3 and N_2O_5 after sunset, mainly in the middle stratosphere (Brasseur and Solomon, 2005). Figure 13 shows a slightly different, but more standard diagnostic of NO_2 A to D ratios for March, and they vary according to the local times of the measurements. However, note that the LIMS observations occurred beyond the day/night terminator at the highest latitudes. V6 NO_2 has low S/N below about the 30-hPa level and is not accurate there; elsewhere the A to D ratios should be representative.

398

399 V6 NO₂ is also sensitive to temperature bias (Table 1, row 6, and Remsberg et al., 2010). Fig. 13
400 shows a slight asymmetry of the 0.7 contour about the equator; that ratio are smaller in the
401 northern subtropics or opposite in magnitude to that expected from the effects of the T(p) bias in
402 Fig. 4. There is significant interfering radiance from H₂O in the NO₂ channel from the middle to
403 ~~the~~ lower stratosphere (Russell et al., 1984), and recall that H₂O has its own T(p) bias effects (see
404 Fig. 9). Radiance from H₂O is also a larger correction for day versus night V6 NO₂. Thus,
405 although we expected to find temperature bias effects in V6 NO₂, indications of them are
406 somewhat ambiguous in Fig. 13.

407

408 **5 Ozone comparisons with rocket-borne measurements**

409 This section considers the quality of the V6 ascending (daytime) ozone of the middle and upper
410 stratosphere at NH middle latitudes; there is only one corresponding comparison for the
411 descending (nighttime) ozone (not shown, but see Remsberg et al., 1984, their Fig. 13). Krueger
412 (1973) developed meteorological rocket-borne, UV-absorption ozonesonde (ROCOZ)
413 instruments in the 1960s and 1970s and made routine soundings of middle atmosphere ozone.
414 To measure absorption of sunlight in three altitude regions between 15 and 60 km, ROCOZ used
415 four interference filters procured commercially in batches for uniformity. There were launches
416 of ROCOZ instruments for the validation of LIMS (seven flights) and of SBUV ozone at low-
417 (Natal, Brazil), mid- (Wallops Island, VA) and high- (Fort Churchill and Primrose Lake,
418 Canada) latitudes. Remsberg et al. (1984) reported on comparisons of the V5 ozone with
419 ROCOZ soundings and found mean differences (V5 minus ROCOZ) that varied from 5% in the
420 upper stratosphere to 16% in the lower stratosphere. The RMS differences were rather large
421 though (12% to 23%, respectively), and there were concerns about the stability of the batch of
422 UV interference filters used in the ROCOZ instruments from late 1978 through mid-1979.

423

424 An early ‘ozone climatology’ was produced from the greater than 200 ROCOZ soundings
425 launched between 1965 and 1990 at rocket ranges from the equator to high latitudes of both
426 hemispheres (Krueger, 1984; WOUDC). The ROCOZ flights include a SH latitude survey,

calibration flights for the Orbital Geophysical Observatory (OGO-4) UV spectrometer (London et al., 1977), low latitude baseline flights from Antigua, high latitude flights from Fort Churchill and Primrose Lake, validation flights for the Backscatter Ultraviolet (BUV) experiment on Nimbus 4, and a regular monthly series of measurements from Wallops Island, VA. In fact, the 1976 U.S. Standard Atmosphere mid-latitude ozone model makes use of rocket data from seven international experimenters, including ROCOZ (Krueger and Minzner, 1976).

Krueger (1984) also compiled separate monthly averages of soundings from Wallops Island (38°N) during the period of March 1976 through September 1978. Uncertainty about the UV filters was not at issue for those soundings. As an example, Fig. 14 compares the April average from ROCOZ with the monthly zonal mean V6 Level 3 daytime ozone at 38°N for April 1979, when wave activity and zonal variations about the V6 daily zonal means are <3%. Even though the V6 profiles contain 18 values per decade of pressure (spaced ~0.88 km), we plot only every other point because the V6 data carry an effective vertical resolution of ~3.7 km. The horizontal bars at 0.3, 1, 2, and 10 hPa represent estimates of bias error for V6 ozone from Remsberg et al. (2007, their Table 1). The ROCOZ profiles are averages of the three April soundings for 1976-1978, and the horizontal bars at 0.5, 1.5, 3, 7, and 15 hPa are their estimated uncertainty of <10% (or <7% for ozone number density versus altitude, plus <3% for the conversion to mixing ratio versus pressure, as taken from Table II-7 of Krueger (1984)). Fig. 14 indicates agreement to within the estimates of bias error for V6 ozone at most altitudes of the stratosphere. V6 ozone is higher than ROCOZ ozone from ~2.0 to 0.3 hPa.

Figure 15 shows V6 daytime minus ROCOZ average profiles at Wallops Island (38°N) for November, March, April, and May. The ozone differences are within their combined error estimates for the middle stratosphere but are larger in the upper stratosphere and, especially, the mesosphere. The increasingly positive, V6 day minus ROCOZ differences in the lower mesosphere from winter to late spring are due to uncorrected NLTE effects for V6 from CO₂ and ozone that increase toward lower solar zenith angles (Solomon et al., 1986; Mlynczak and Drayson, 1990). On the other hand, the V6 daytime ozone of April and May is also larger than ROCOZ ozone at 1.5 to 3 hPa, where NLTE should not be an issue (Edwards et al., 1996).

457 While there may be excess V6 ozone due to a slight negative bias for V6 T(p) at those pressure-
458 altitudes, it may also be that the ROCOZ climatology at Wallops Islands is not truly
459 representative of zonal average ozone for those months of 1979. In the next section, we report
460 on time series of fields of potential vorticity, ozone, and H₂O from their V6 Level 3 combined
461 (A+D) products for the middle stratosphere, where those parameters are not expected to have
462 diurnal variations and should serve as tracers of atmospheric transport.

463

464 **6 Seasonal transport of V6 ozone and water vapor**

465 Dunkerton and DeLisi (1986) made use of LIMS V5 GPH and temperature data to calculate
466 potential vorticity (PV) and then to show how PV evolved in the NH on the 850 K potential
467 temperature (~10 hPa) surface during January and February 1979. Butchart and Remsberg (BR,
468 1986) also calculated PV from the V5 data and plotted its evolution during the winter of 1978-
469 1979 in terms of the fractional area of the NH enclosed by the horizontal projection of a given
470 PV contour on the 850 K surface. These so-called, area diagnostic analyses of BR work well for
471 a parameter like PV that is monotonic with latitude, having its highest value at the Pole.

472

473 New time series analyses of PV from the combined V6 data are in Fig. 16, calculated from the
474 Level 3, daily 6-wavenumber, zonal coefficients of GPH and temperature. Equivalent latitude
475 (on the right ordinate) represents the latitude at which a zonally symmetric PV contour would lie
476 if it enclosed the given fractional area shown on the left ordinate. PV data for Fig. 16 have a 7-
477 day smoothing, and the NH fractional area extends only to 20° equivalent latitude because
478 calculations of absolute vorticity are not so accurate near the Equator. The PV results for V6 are
479 nearly identical to those for V5 in BR (their Fig. 4). Notably, the polar vortex (defined by
480 highest PV values) erodes during winter and the adjacent ‘surf-zone’, having much lower PV
481 gradients, expands in area due to the ‘breaking’ of planetary waves and the associated meridional
482 mixing of vortex and lower latitude air.

483

484 Ozone is an effective tracer of the transport of air in and around the winter polar vortex on the
485 850 K surface (~10 hPa) (Leovy et al., 1985). Ozone also varies nearly monotonically at this
486 level, but with highest values at low latitudes and lowest values near the Pole. BR analyzed the
487 evolution of V5 ozone (see their Fig. 10b). They compared its changes with those of PV and
488 found good correspondence for the large-scale features of the two distributions. Fig. 17 is the
489 new ozone time series at 850 K from the gridded V6 data, and it compares well with the
490 calculations of BR from the V5 ozone. One significant change with V6 is that the ozone
491 contours of 6.8 through 7.2 ppmv of early February indicate very weak gradients within the surf
492 zone, as it expands following the major warming event of late January. There is also an
493 associated, diabatic cross-isentropic transport of ozone within the surf zone during that time
494 (e.g., Butchart, 1987). The improved continuity of the ozone time series from V6 is a result of
495 the better spatial sampling for the radiances, of the retrievals of T(p) profiles, and of the
496 corresponding changes for the registration of the ozone radiance profiles and retrieved ozone
497 mixing ratios.

498
499 Water vapor is also a tracer of the net transport in the middle stratosphere. Figure 18 shows the
500 corresponding time series of V6 H₂O at 850 K. V6 H₂O mixing ratio contours vary more
501 smoothly than those from the V5 data in BR (their Fig. 12); the retrieved V6 H₂O profiles are
502 better resolved spatially and have better precision. There is good correspondence between H₂O,
503 PV, and ozone for the location and evolution of the edge of the polar winter vortex and for the
504 expansion of the region of weak gradients at middle latitudes. Low values of H₂O extend to the
505 northern middle latitudes and high values of H₂O descend within the polar vortex from
506 November through January, indicating an acceleration of the Brewer/Dobson circulation during
507 that winter. There is also a modest expansion of weak H₂O gradients between 40°N to 60°N
508 equivalent latitude from mid-November to mid-December. This region coincides with the time
509 of the Canadian warming and an exchange of air between polar and middle latitudes.

510

511 **7 Summary and recommendations**

512 This study provides some insight about the quality of the LIMS V6 Level 3 product and about
513 the generation of daily gridded species distributions on pressure surfaces. Monthly zonal mean
514 distributions are available within the SPARC-DI database for comparisons with model
515 simulations of middle atmosphere species. We also provide the corresponding monthly zonal
516 mean distributions of temperature for SPARC-DI and diagnostic evidence of effects of residual
517 temperature biases in the V6 ozone, H₂O, and HNO₃ distributions. Those species exhibit
518 ascending minus descending (A-D or day minus night at most latitudes) anomalies, especially in
519 the middle and lower stratosphere. In particular, the A-D ozone and H₂O values are larger than
520 expected due to not accounting for all of the horizontal temperature structure, which affects
521 forward radiance calculations through the Planck blackbody function, the retrievals of T(p), and
522 the registration of species radiance profiles with pressure. It may be that the V6 species
523 distributions within the SH have better accuracy from along its ascending (A) orbital segments,
524 since the tangent view paths for its profiles are more nearly in a zonal direction and do not have
525 significant T(p) gradients. Finally, we found no clear evidence of temperature bias in V6 NO₂.

526
527 Remsberg et al. (2013) reported that an assimilation of SBUV ozone along with the V6 A and D
528 Level 2 ozone profiles provides ozone distributions that agree well with balloon-sonde ozone in
529 the lower stratosphere. Yet, we do not recommend assimilation studies based on only the V6
530 ozone profiles because of their small, but persistent A-D differences, particularly at the edge of
531 and within the winter polar vortex. V6 H₂O profiles present similar assimilation problems.
532 Instead, we recommend that researchers make use of the average (A+D) V6 Level 3 product
533 and/or the SPARC-DI monthly, zonal average distributions for their science studies of
534 stratospheric ozone and H₂O, at least where NLTE effects are not an issue. As an example,
535 Tegtmeier et al. (2013) compared the combined V6 monthly stratospheric ozone distributions
536 with ones from other satellite-based limb sensors, and they found good agreement. Thereafter,
537 Shepherd et al. (2014) integrated the SPARC-DI V6 monthly zonal mean ozone above the
538 tropopause and subtracted it from observed total ozone as part of their assessment of long-term
539 trends of tropospheric ozone from models for 1978 and onward.

540

541 Remsberg et al. (2007, their Fig. 8b) found that zonal average V6 ozone in the middle
542 stratosphere is higher than SBUV ozone by 4%, which is well within the combined systematic
543 errors of both experimental datasets. Correlative ozone measurements for the middle to upper
544 stratosphere are too few and too inaccurate in 1978/1979 to determine whether the V6 A or D
545 ozone is more accurate. Thus, we considered V6 monthly profile data versus a monthly daytime
546 ozone climatology of the late 1970s obtained with the rocket-borne, uv-absorption (ROCOZ)
547 technique at Wallops Island, VA. We found agreement within their respective errors, except for
548 the uppermost stratosphere and the lower mesosphere. We also calculated time series of V6
549 Level 3 ozone and H₂O at 850 K and looked for consistency between their fields and those of
550 PV. In general, we found good agreement with similar studies of BR (1986) based on V5 data.
551 However, the time series from V6 show s better continuity during dynamically active periods.

552
553 The LIMS experience has been of benefit for the design of follow-on broadband, limb infrared
554 measurements. One satellite experiment, the Sounding of the Atmosphere using Broadband
555 Emission Radiometry (SABER), has been obtaining measurements of temperature, ozone, and
556 H₂O from 2002-2020 (e.g., Remsberg et al., 2008; Rong et al., 2009). Improvements from
557 SABER compared to LIMS are: (1) reductions in electronics and detector noise for its narrow-
558 band and wide-band CO₂ channels by factors of 5 and 16, respectively, and for its ozone channel
559 by a factor of 20; (2) common, 2-km IFOVs for its CO₂ (for temperature) and species channels to
560 account for diurnal temperature signals in the retrievals of ozone and H₂O; (3) an ozone filter
561 bandpass of about 1000 to 1150 cm⁻¹ to avoid the NLTE emissions from the CO₂ laser band at
562 960 cm⁻¹; and (4) NLTE algorithms for retrievals of T(p), ozone, and H₂O in the mesosphere.
563 SABER instrument operation is stable and its orbital attitude information is accurate (Mlynczak
564 et al., 2020). SABER tangent view paths are 90° away from the spacecraft velocity vector or in
565 nearly a zonal direction for the low and middle latitudes, where zonal temperature gradients are
566 weak. There is little need to correct for T(p) gradients in the SABER algorithms, except when
567 viewing the high latitudes. Accordingly, diurnal temperature and ozone variations from SABER
568 compare reasonably with those from microwave measurements and with model estimates (e.g.,
569 Huang et al., 2010a and 2010b; Frith et al., 2020).

571 **Data Availability**

572 The LIMS V6 data archive is at the NASA EARTHDATA site of EOSDIS and its website:
573 <https://search.earthdata.nasa.gov/search?q=LIMS>). The ROCOZ ozone climatology at Wallops
574 Island is available from co-author, Arlin Krueger, upon request. The SPARC-Data Initiative site
575 is located at <https://www.sparc-climate.org/data-centre/data-access/sparc-data-initiative/>. We
576 acknowledge the individual instrument teams and respective space agencies for making their
577 measurements available, and the Data Initiative of WCRP's (World Climate Research
578 Programme) SPARC (Stratospheric Processes and their Role in Climate) project for organizing
579 and coordinating the compilation of the chemical trace gas datasets used in this work.

580

581 *Author Contributions.* ER prepared most of the figures and wrote the manuscript with
582 contributions from all co-authors. MN produced plots of the ascending minus descending
583 radiances. VLH prepared the time series plots of PV, ozone, and H₂O. AK provided his early
584 rocketsonde data on ozone and temperature and their estimated errors.

585

586 *Acknowledgements.* We are grateful to Krzysztof Wargan, who communicated to author ER in
587 2017 that he had concerns about the assimilation of alternating V6 A and D polar ozone profiles
588 during a re-analysis run of the MERRA model. We especially thank John Burton, L. L. Gordley,
589 B. T. Marshall, and R. E. Thompson for producing the V6 Level 2 dataset. Gretchen
590 Lingenfelser generated the V6 Level 3 zonal Fourier coefficient data. We thank John Gille and
591 Ernest Hilsenrath, who read and commented on a draft version of the manuscript. VLH
592 acknowledges support from NSF CEDAR grant 1343031, NASA LWS grant NNX14AH54G,
593 NASA HGI grant NNX17AB80G, and from NASA HSR grant 80NSSC18K1046. ER and MN
594 carried out their work while serving as a Distinguished Research Associates of the Science
595 Directorate at NASA Langley.

References

- Barnett, J., and Corney, M.: Middle atmosphere reference model derived from satellite data, in Handbook for Middle Atmosphere Program, Labitzke, K, Barnett, J. J., and Edwards, B., (Eds.), vol. 16, 47-137, NASA Contractor Report 176321, Document ID 19860003346, <https://ntrs.nasa.gov>, (last access November 12, 2019), 1985.
- Brasseur, G., and Solomon, S.: Aeronomy of the Middle Atmosphere: Chemistry and Physics of the Stratosphere and Mesosphere. 3rd ed., 644 pp., Springer, Dordrecht, Netherlands, 2005.
- Butchart, N.: Evidence for planetary wave breaking from satellite data: the relative roles of diabatic effects and irreversible mixing, in *Transport Processes in the Middle Atmosphere*, Visconti, G., and Garcia, R. (Eds.), D. Reidel Publishing Co., Dordrecht, Holland, pp. 121-136, 1987.
- Butchart, N. and Remsberg, E. E.: The area of the stratospheric polar vortex as a diagnostic for tracer transport on an isentropic surface, J. Atmos. Sci., 43, 1319-1339, [https://doi.org/10.1175/1520-0469\(1986\)043%3C1319:TAOTSP%3E2.0.CO;2](https://doi.org/10.1175/1520-0469(1986)043%3C1319:TAOTSP%3E2.0.CO;2), 1986.
- Dunkerton, T. J. and DeLisi, D. P.: Evolution of potential vorticity in the winter stratosphere of January-February 1979, J. Geophys. Res. 91, 1199-1208, <https://doi.org/10.1029/JD091iD01p01199>, 1986.
- Edwards, D. P., Kumer, J. B., Lopez-Puertas, M., Mlynchak, M. G., Gopalan, A., Gille, J. C., and Roche, A.: Non-local thermodynamic equilibrium limb radiance near 10 μm as measured by UARS CLAES, J. Geophys. Res., 101, D21, 26,577-26,588, <https://doi.org/10.1029/96JD02133>, 1996.

623 Finger, F. G., Gelman, M. E., Schmidlin, F. J., Leviton, R., and Kennedy, V. W.: Compatibility
 624 of meteorological rocketsonde data as indicated by international comparisons tests, J. Atmos.
 625 Sci., 32, 1705-1714, [https://doi.org/10.1175/1520-
 626 0469\(1975\)032%3C1705:COMRDA%3E2.0.CO;2](https://doi.org/10.1175/1520-0469(1975)032%3C1705:COMRDA%3E2.0.CO;2), 1975.

627

628 Frith, S. M., Bhartia, P. K., Oman, L. D., Kramarova, N. A., McPeters, R. D., and Labow, G. J.:
 629 Model-based climatology of diurnal variability in stratospheric ozone as a data analysis tool,
 630 Atmos. Meas. Tech., 13, 2733-2749, <https://doi.org/10.5194/amt-13-2733-2020>, 2020.

631

632 Gille, J. C. and Russell III, J. M.: The limb infrared monitor of the stratosphere: experiment
 633 description, performance, and results, J. Geophys. Res., 84, 5125-5140,
 634 <https://doi.org/10.1029/JD089iD04p05125>, 1984.

635

636 Gille, J. C., Russell III, J. M., Bailey, P. L., Gordley, L. L., Remsberg, E. E., Lienesch, J. H.,
 637 Planet, W. G., House, F. B., Lyjak, L. V., and Beck, S. A.: Validation of temperature retrievals
 638 obtained by the limb infrared monitor of the stratosphere (LIMS) experiment on NIMBUS 7, J.
 639 Geophys. Res., 89, 5147-5160, <https://doi.org/10.1029/JD089iD04p05147>, 1984.

640

641 Gordley, L. L. and Russell, J. M.: Rapid inversion of limb radiance data using an emissivity
 642 growth approximation, Appl. Opt., 20, 807-813, <https://doi.org/10.1364/AO.20.000807>, 1981.

643

644 Haigh, J. D., and Pyle, J. A.: Ozone perturbation experiments in a two-dimensional circulation
 645 model, Q. J. Roy. Meteorol. Soc., 108, 551-574, <https://doi.org/10.1002/qj.49710845705>, 1982.

646

647 Hitchman, M. H., and Leovy, C. B.: Diurnal tide in the equatorial middle atmosphere as seen in
 648 LIMS temperatures, J. Atmos. Sci., 42, 557-561, [https://doi.org/10.1175/1520-
 649 0469\(1985\)042%3C0557:DTITEM%3E2.0.CO;2](https://doi.org/10.1175/1520-0469(1985)042%3C0557:DTITEM%3E2.0.CO;2), 1985.

650

651 Huang, F. T., McPeters, R. D., Bhartia, P. K., Mayr, H. G., Frith, S. M., Russell III, J. M., and
652 Mlynczak, M. G.: Temperature diurnal variations (migrating tides) in the stratosphere and lower
653 mesosphere based on measurements from SABER on TIMED, *J. Geophys. Res.*, 115, D16121,
654 [https://doi:10.1029/2009JD013698](https://doi.org/10.1029/2009JD013698), 2010a.

655

656 Huang, F. T., Mayr, H. G., Russell III, J. M., and Mlynczak, M. G.: Ozone diurnal variations in
657 the stratosphere and mesosphere, based on measurements from SABER on TIMED, *J. Geophys.*
658 *Res.*, 115, D24308, [https://doi:10.1029/2010JD014484](https://doi.org/10.1029/2010JD014484), 2010b.

659

660 Kiefer, M., Arnone, E., Dudhia, A., Carlotti, M., Castelli, E., von Clarmann, T., Dinelli, B. M.,
661 Kleinert, A., Linden, A., Milz, M., Papandrea, E., and Stiller, G.: Impact of temperature field
662 inhomogeneities on the retrieval of atmospheric species from MIPAS IR limb emission spectra,
663 *Atmos. Meas. Tech.*, 3, 1487–1507, <https://doi.org/10.5194/amt-3-1487-2010>, 2010.

664

665 Krueger, A. J.: The mean ozone distribution from several series of rocket soundings to 52 km at
666 latitudes from 58°S to 64°N, *PAGEOPH*, 106, 1272-1280, <https://doi.org/10.1007/BF00881079>,
667 1973.

668

669 Krueger, A. J: Inference of photochemical trace gas variations from direct measurements of
670 ozone in the middle atmosphere, Doctoral Dissertation, Colorado State Univ., Fort Collins, CO,
671 1984, (available for download from ResearchGate:
672 [https://www.researchgate.net/publication/253654486_Inference_of_photochemical_trace_gas_va](https://www.researchgate.net/publication/253654486_Inference_of_photochemical_trace_gas_variations_from_direct_measurements_of_ozone_in_the_middle_atmosphere)
673 [riations_from_direct_measurements_of_ozone_in_the_middle_atmosphere](https://www.researchgate.net/publication/253654486_Inference_of_photochemical_trace_gas_variations_from_direct_measurements_of_ozone_in_the_middle_atmosphere)).

674

675 Krueger, A. J. and Minzner, R. A.: A mid-latitude ozone model for the 1976 U. S. standard
 676 atmosphere, J. Geophys. Res., 81, 4477-4481, <https://doi.org/10.1029/JC081i024p04477>,
 677 1976.
 678
 679 Leovy, C. B., Sun, C-R., Hitchman, M. H., Remsberg, E. E., Russell, III, J. M., Gordley, L. L.,
 680 Gille, J. C., and Lyjak, L. V.: Transport of ozone in the middle stratosphere: evidence for
 681 planetary wave breaking, J. Atmos. Sci., 42, 230-244, [https://doi.org/10.1175/1520-0469\(1985\)042%3C0230:TOOITM%3E2.0.CO;2](https://doi.org/10.1175/1520-0469(1985)042%3C0230:TOOITM%3E2.0.CO;2), 1985.
 682
 683
 684 London, J., Frederick, J. E., and Anderson, G. P.: Satellite observations of the global distribution
 685 of stratospheric ozone, J. Geophys. Res., 82, 2543-2556,
 686 <https://doi.org/10.1029/JC082i018p02543>, 1977.
 687
 688 Lopez-Puertas, M. and Taylor, F. W.: Non-LTE Radiative transfer in the Atmosphere, World
 689 Scientific Publ. Co., River Edge, NJ, USA, 504 pp., 2001.
 690
 691 Manuilova, R. O., Gusev, O. A., Kutepov, A. A., von Clarmann, T., Oelhaf, H., Stiller, G. P.,
 692 Wegner, A., Lopez-Puertas, M., Martin-Torres, F. J., Zaragoza, G., and Flaud, J.-M.: Modelling
 693 of non-LTE limb spectra of i.r. ozone bands for the MIPAS space experiment, J. Quant.
 694 Spectrosc. Rad. Transf., 59, 405-422, [https://doi.org/10.1016/S0022-4073\(97\)00120-9](https://doi.org/10.1016/S0022-4073(97)00120-9), 1998.
 695
 696 Mertens, C. J., Mlynchak, M. G., Lopez-Puertas, M., and Remsberg, E. E.: Impact of non-LTE
 697 processes on middle atmospheric water vapor retrievals from simulated measurements of 6.8 μm
 698 Earth limb emission, Geophys. Res. Lett., 29 (9), 2-1 to 2-4,
 699 <https://doi.org/10.1029/2001GL014590>, 2002.
 700

701 Mlynczak, M. G., Daniels, T., Hunt, L. A., Yue, J., Marshall, B. T., Russell, J. M., III,
702 Remsberg, E. E., Tansock, J., Esplin, R., Jensen, M., Shumway, A., Gordley, L., and Yee, J.-H.:
703 Radiometric stability of the SABER instrument. *Earth and Space Science*, 7, e2019EA001011,
704 <https://doi.org/10.1029/2019EA001011>, 2020.

705

706 Mlynczak, M. G. and Drayson, R.: Calculation of infrared limb emission by ozone in the
707 terrestrial middle atmosphere 2. Emission calculations, *J. Geophys. Res.*, 95, 16,513-16,521,
708 <https://doi.org/10.1029/JD095iD10p16513>, 1990.

709

710 Remsberg, E., and Lingenfelter, G.: LIMS Version 6 Level 3 dataset, NASA-TM-2010-216690,
711 available at <http://www.sti.nasa.gov> (last access: 17 September 2019), 13 pp., 2010.

712

713 Remsberg, E. E., Haggard, K. V., & Russell, J. M., III. (1990). Estimation of Synoptic Fields of
714 Middle Atmosphere Parameters from Nimbus-7 LIMS Profile Data. *Journal of Atmospheric and*
715 *Oceanic Technology*, 7(5), 689-705. Retrieved Jan 28, 2021,
716 from [https://journals.ametsoc.org/view/journals/atot/7/5/1520-](https://journals.ametsoc.org/view/journals/atot/7/5/1520-0426_1990_007_0689_eosfom_2_0_co_2.xml)
717 [0426_1990_007_0689_eosfom_2_0_co_2.xml](https://journals.ametsoc.org/view/journals/atot/7/5/1520-0426_1990_007_0689_eosfom_2_0_co_2.xml), 1990,

Formatted: Font: (Default) Times New Roman, 12 pt

Formatted: Font: (Default) Times New Roman, 12 pt

Formatted: Font: (Default) Times New Roman, 12 pt

Formatted: Font: (Default) Times New Roman, 12 pt

Formatted: Font: (Default) Times New Roman, 12 pt

718

719 Remsberg, E. E., Russell, J. M., III, Gille, J. C., Bailey, P. L., Gordley, L. L., Planet, W. G., and
720 Harries, J. E.: The validation of Nimbus 7 LIMS measurements of ozone, *J. Geophys. Res.*, 89,
721 5161-5178, <https://doi.org/10.1029/JD089iD04p05161>, 1984.

722

723 Remsberg, E. E., Gordley, L. L., Marshall, B. T., Thompson, R. E., Burton, J., Bhatt, P., Harvey,
724 V. L., Lingenfelter, G., Natarajan, M.: The Nimbus 7 LIMS version 6 radiance conditioning and
725 temperature retrieval methods and results, *J. Quant. Spectros. Rad. Transf.*, 86, 395-424,
726 <https://doi.org/10.1016/j.jqsrt.2003.12.007>, 2004.

727

728 Remsberg, E., Lingenfelser, G., Natarajan, M., Gordley, L., Marshall, B. T., and Thompson, E.:
729 On the quality of the Nimbus 7 LIMS version 6 ozone for studies of the middle atmosphere, J.
730 Quant. Spectros. Rad. Transf., 105, 492-518, <https://doi.org/10.1016/j.jqsrt.2006.12.005>, 2007.

731
732 Remsberg, E. E., Marshall, B. T., Garcia-Comas, M., Krueger, D., Lingenfelser, G. S., Martin-
733 Torres, J., Mlynczak, M. G., Russell III, J. M., Smith, A. K., Zhao, Y., Brown, C., Gordley, L.
734 L., Lopez-Gonzalez, M. J., Lopez-Puertas, M., She, C. Y., Taylor, M. J., and Thompson, E.:
735 Assessment of the quality of the Version 1.07 temperature versus pressure profiles of the middle
736 atmosphere from TIMED/SABER, J. Geophys. Res., 113, D17101,
737 <https://doi.org/10.1029/2008JD010013>, 2008.

738
739 Remsberg, E. E., Natarajan, M., Lingenfelser, G. S., Thompson, R. E., Marshall, B. T., and
740 Gordley, L. L.: On the quality of the Nimbus 7 LIMS Version 6 water vapor profiles and
741 distributions, Atmos. Chem. Phys., 9, 9155-9167, www.atmos-chem-phys.net/9/9155/2009/,
742 2009.

743
744 Remsberg, E., Natarajan, M., Marshall, B. T., Gordley, L. L., Thompson, R. E., and
745 Lingenfelser, G. S.: Improvements in the profiles and distributions of nitric acid and
746 nitrogen dioxide with the LIMS version 6 dataset, Atmos. Chem. Phys., 10, 4741–4756,
747 www.atmos-chem-phys.net/10/4741/2010/, 2010.

748
749 Remsberg, E., Natarajan, M., Fairlie, T. D., Wargan, K., Pawson, S., Coy, L., Lingenfelser, G.,
750 and Kim, G.: On the inclusion of Limb Infrared Monitor of the Stratosphere version 6 ozone in a
751 data assimilation system, J. Geophys. Res., 118, 7982-8000, <https://doi.org/10.1002/jgrd.50566>,
752 2013.

753

754 Roewe, D. A., Gille, J. C., and Bailey, P. L.: Infrared limb scanning in the presence of horizontal
 755 temperature gradients: an operational approach, *Appl. Opt.*, 21, 3775-3783,
 756 <http://dx.doi.org/10.1364/AO.21.003775>, 1982.
 757
 758 Rong, P. P., Russell III, J. M., Mlynczak, M. G., Remsberg, E. E., Marshall, B. T., Gordley, L.
 759 L., and Lopez-Puertas, M.: Validation of Thermosphere Ionosphere Mesosphere Energetics and
 760 Dynamics/Sounding of the Atmosphere using Broadband Emission Radiometry
 761 (TIMED/SABER) v1.07 ozone at 9.6 μm in altitude range 15–70 km, *J. Geophys. Res.*, 114,
 762 D04306, <https://doi.org/10.1029/2008JD010073>, 2009.
 763
 764 Russell, J. M., III, Gille, J. C., Remsberg, E. E., Gordley, L. L., Bailey, P. L., Drayson, S. R.,
 765 Fischer, H., Girard, A., Harries, J. E., and Evans, W. F. J.: Validation of nitrogen dioxide results
 766 measured by the Limb Infrared Monitor of the Stratosphere (LIMS) experiment on Nimbus 7, *J.*
 767 *Geophys. Res.*, 89, 5099-5107, <https://doi.org/10.1029/JD089iD04p05099>, 1984.
 768
 769 Sakazaki, T., Fujiwara, M., Mitsuda, C., Imai, K., Manago, N., Naito, Y., Nakamura, T.,
 770 Akiyoshi, H., Kinnison, D., Sano, T., Suzuki, M., and Shiotani, M.: Diurnal ozone variations in
 771 the stratosphere revealed in observations from the Superconducting Submillimeter-Wave Limb-
 772 Emission Sounder (SMILES) on board the International Space Station (ISS), *J. Geophys. Res.*,
 773 118, 2991-3006, <https://doi.org/10.1002/jgrd.50220>, 2013.
 774
 775 Shepherd, T. G., Plummer, D. A., Scinocca, J. F., Hegglin, M. I., Fioletov, V. E., Reader, M. C.,
 776 Remsberg, E., von Clarmann, T., and Wang, H. J.: Reconciliation of halogen-induced ozone loss
 777 with the total-column record, *Nature Geoscience*, 7, 443-449, <https://doi.org/10.1038/ngeo2155>,
 778 2014.
 779

780 Solomon, S., Kiehl, J. T., Kerridge, B. J., Remsberg, E. E., and Russell III, J. M.: Evidence for
781 nonlocal thermodynamic equilibrium in the ν_3 mode of mesospheric ozone, J. Geophys. Res.,
782 91, 9865-9876, <https://doi.org/10.1029/JD091iD09p09865>, 1986.

783

784 SPARC: The SPARC Data Initiative: Assessment of stratospheric trace gas and aerosol
785 climatologies from satellite limb sounders, Hegglin, M. I. and Tegtmeier, S., (Eds.), SPARC
786 Report No. 8, WCRP-5/2017, <http://www.sparc-climate.org/publications/sparc-reports/>, 2017.

787

788 Sun, C.-R., and Leovy, C.: Ozone variability in the equatorial middle atmosphere, J. Geophys.
789 Res., 95, 13,829-13,849, <https://doi.org/10.1029/JD095iD09p13829>, 1990.

790

791 Tegtmeier, S., Hegglin, M. I., Anderson, J., Bourassa, A., Brohede, S., Degenstein, D.,
792 Froidevaux, L., Fuller, R., Funke, B., Gille, J., Jones, A., Kasai, Y., Krüger, K., Kyrölä, E.,
793 Lingenfelser, G., Lumpe, J., Nardi, B., Neu, J., Pendlebury, D., Remsberg, E., Rozanov, A.,
794 Smith, L., Toohey, M., Urban, J., von Clarmann, T., Walker, K. A. and Wang, R. H. H.: SPARC
795 Data Initiative: A comparison of ozone climatologies from international satellite limb sounders,
796 J. Geophys. Res., 118, 12,229-12,247, <https://doi.org/10.1002/2013JD019877>, 2013.

797

798 WOUDC, World Ozone and Ultraviolet Radiation Data Centre, <https://woudc.org/home.php>.

799

800

801

Table 1

802

Estimates of Species Errors Due to Temperature Biases

803

Pressure (hPa)	100	50	10	3	1	0.4	0.1
Temperature Bias (K)	1.1	1.3	1.0	1.6	2.4	2.5	2.3
Ozone (%)	20	20	11	10	12	16	16
Water vapor (%)	16	18	8	15	--	--	--
Nitric acid (%)	5	1	1	6	--	--	--
Nitrogen Dioxide (%)	--	22	8	6	10	--	--
T(p) Diff (V6-BC) (K)	--	1.4	1.7	-4.4	-1.6	3.1	--

804

805

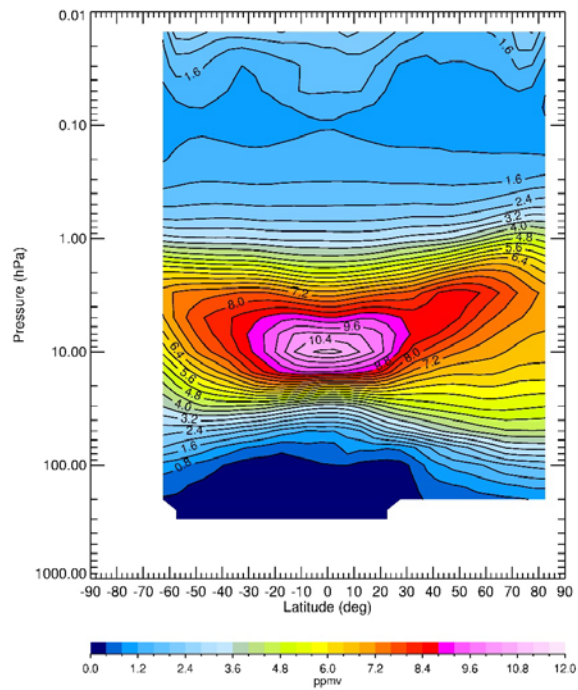
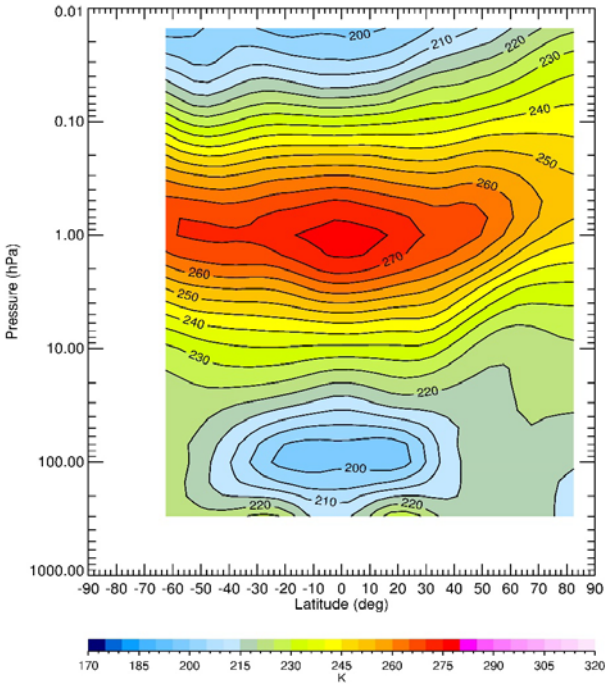


Figure 1—Zonal average ozone for March 1979 from the combination of the LIMS V6 ascending and descending orbital data. Contour interval (CI) is 0.4 ppmv.

813

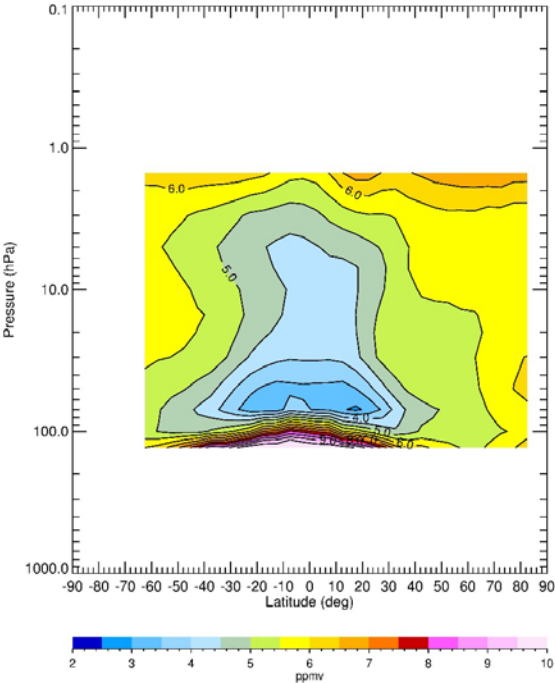


814

815 Figure 2—Zonal average temperature for March 1979. CI is 5 K.

816

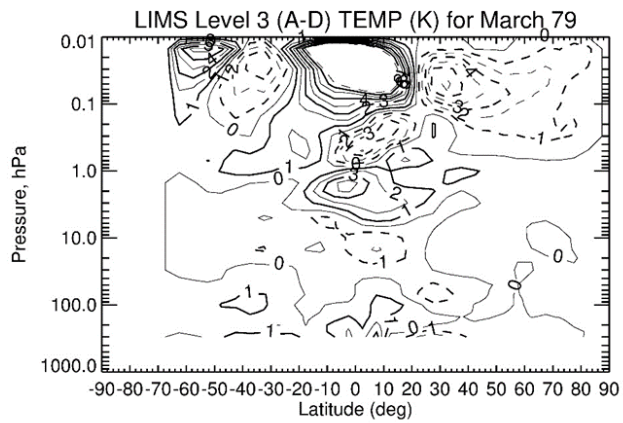
817



818

819 Figure 3—Zonal average water vapor for March 1979. CI is 0.5 ppmv.

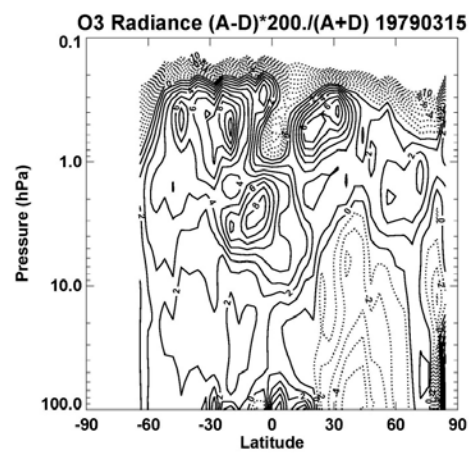
820



821
 822 Figure 4—LIMS V6 Level 3 ascending minus descending (A-D) temperature differences (in K)
 823 for March 1979. CI is 1 K and solid contours show positive differences.

824

825



826

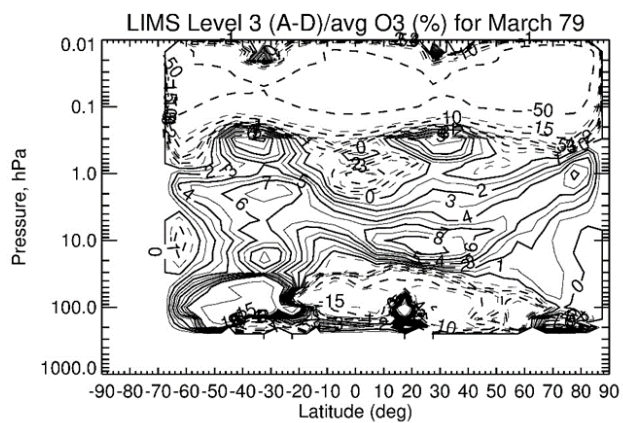
827 Figure 5—Ascending minus descending ozone radiance differences (in %) for March 15, 1979.

828 Contour interval is 1%.

829

830

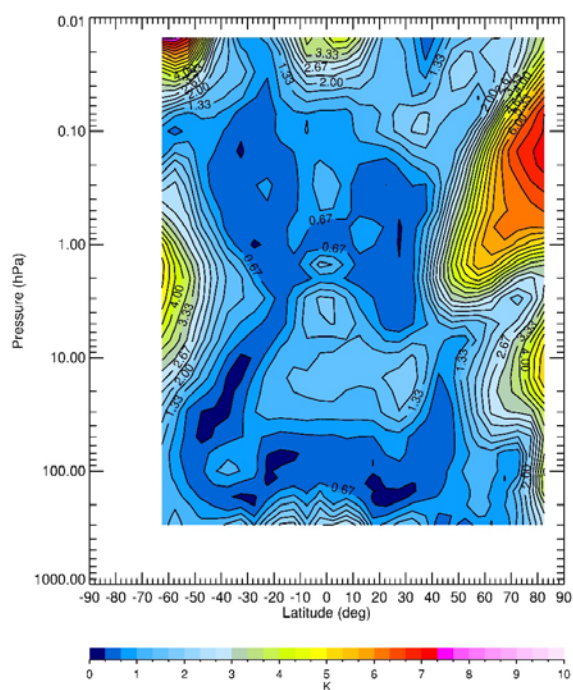
831



832

833 Figure 6—LIMS V6 Level 3 monthly zonal mean (A-D) ozone differences divided by average
834 ozone (and given in %) for March 1979. Solid contours are positive and CI is 1% from 0 to 10,
835 5% from 10 to 15, and then skipping to the 50% contour.

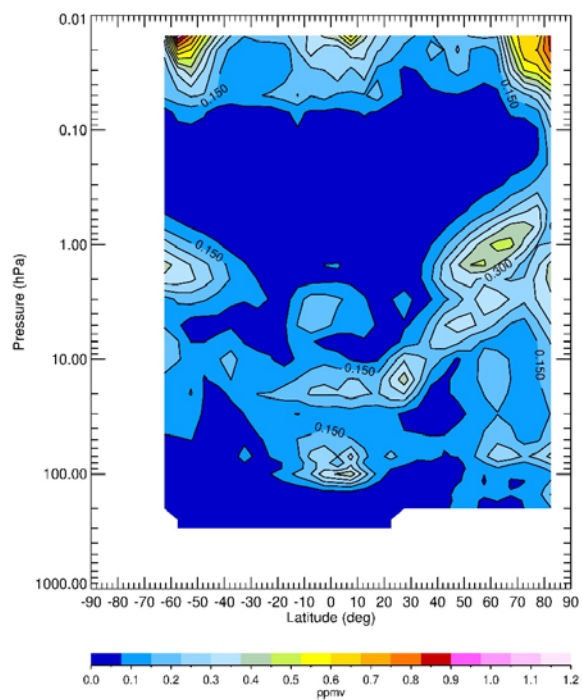
836



837

838 Figure 7—Average zonal (wave) standard deviation of temperature for March 1979. Contour
839 interval is 0.33 K.

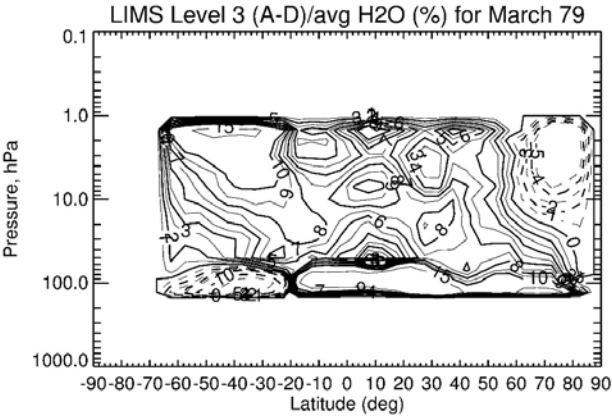
840



841
 842 Figure 8—Average zonal (wave) standard deviation of ozone for March 1979. Contour interval
 843 is 0.075 ppmv.

844

845



846

847 Figure 9—LIMS V6 Level 3 ascending minus descending (A-D) H₂O differences divided by
848 average H₂O (and given in %) for March 1979. CI is 1% from 0 to 10 and then 5% from 10 to
849 15; solid contours show positive differences.

850

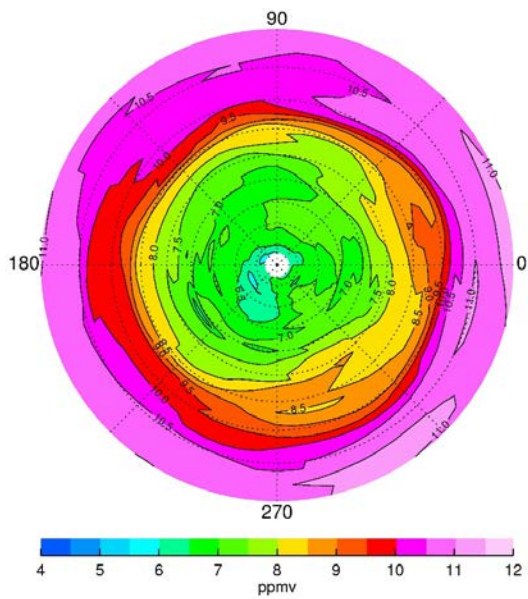
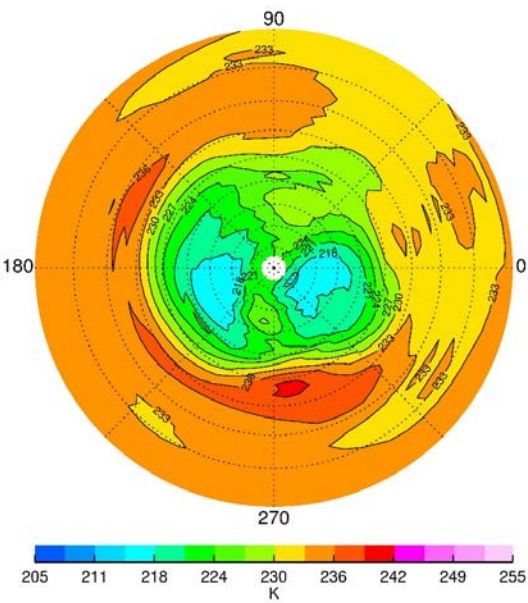


Figure 10—V6 ozone at 10 hPa for March 15, 1979, in the NH. Ozone contour interval is 0.5 ppmv, and latitude spacing (dotted circles) is 10°.

857



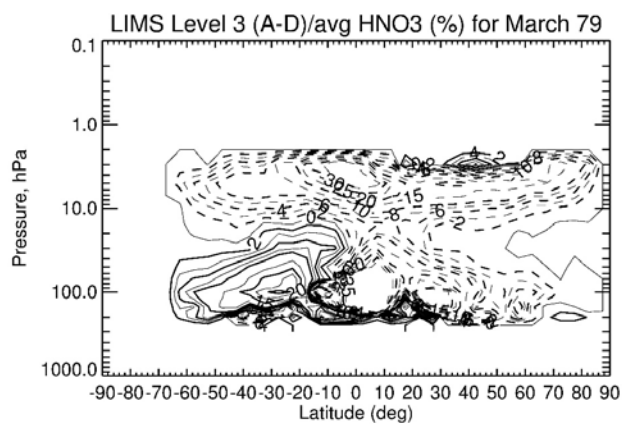
858

859 Figure 11—V6 temperature at 10 hPa for March 15, 1979, in the NH; contour interval is 3 K.

860

861

862

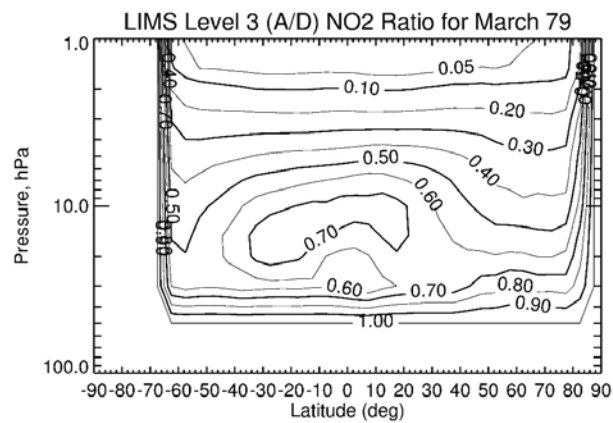


863

864 Figure 12—LIMS V6 Level 3 ascending minus descending (A-D) HNO₃ differences divided by
865 average HNO₃ (and given in %) for March 1979. CI is 2% from 0 to 10 and then 5% from 10 to
866 35; solid contours show positive differences.

867

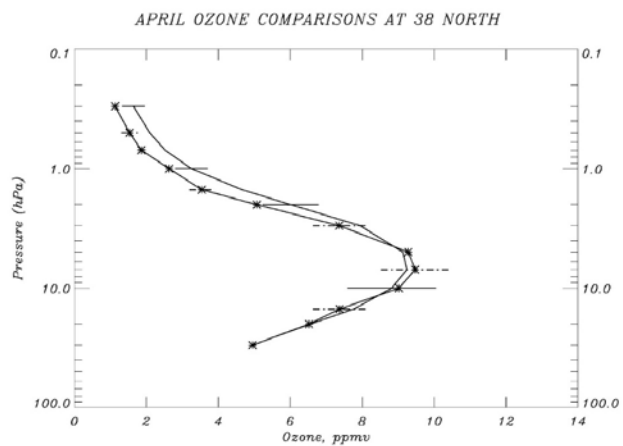
868



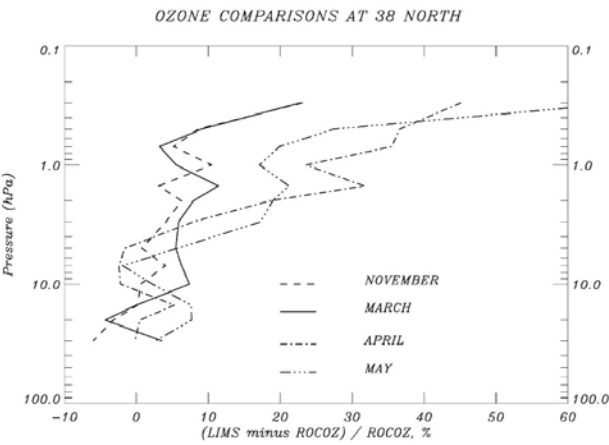
869

870 Figure 13—Distribution of the A to D ratios of V6 NO₂ for March 1979. CI is 0.05 (from 0.0 to
871 0.1) and then 0.1 (from 0.1 to 1.0).

872



879

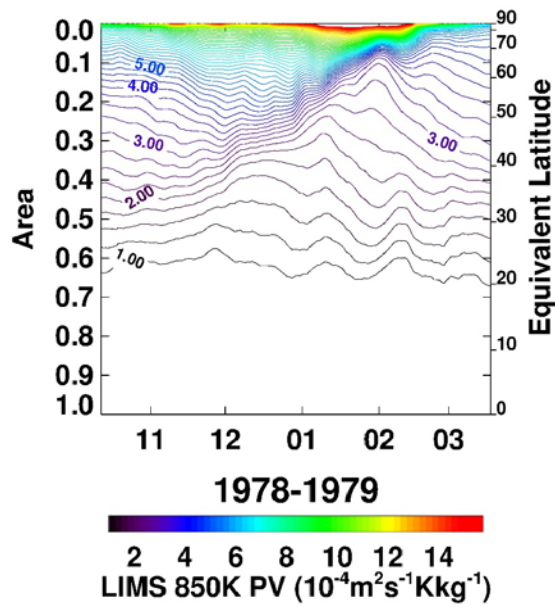


880

881 Figure 15—Monthly zonal mean V6 daytime ozone minus ROCOZ ozone (in %) for four months
882 at 38°N.

883

884

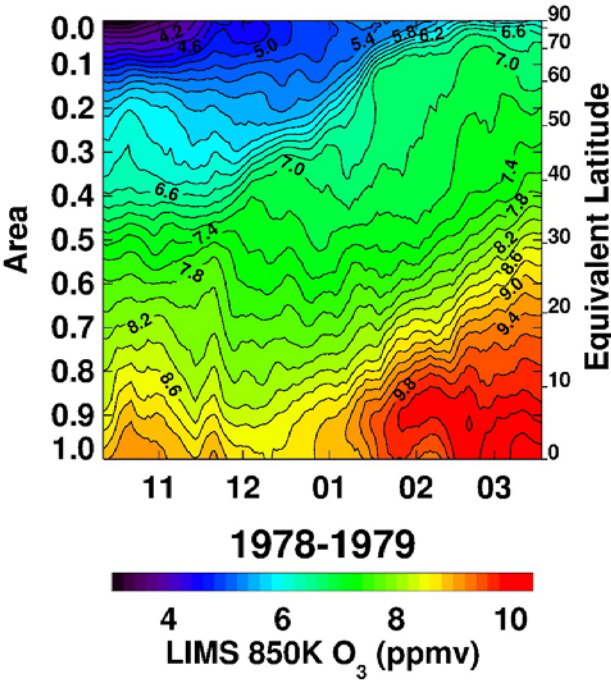


885

886 Figure 16—Area diagnostic plot of time series of NH potential vorticity (PV) contours on the
887 850 K potential temperature surface for comparison with Butchart and Remsberg (1986, their
888 Figure 4). PV comes from LIMS V6 Level 3 geopotential height and temperature data. Contour
889 interval (CI) is 0.25 PV units (units of PV are $10^{-4} \text{ m}^2 \text{ s}^{-1} \text{ K kg}^{-1}$). Tic marks on the abscissa
890 denote the 15th of each month.

891

892

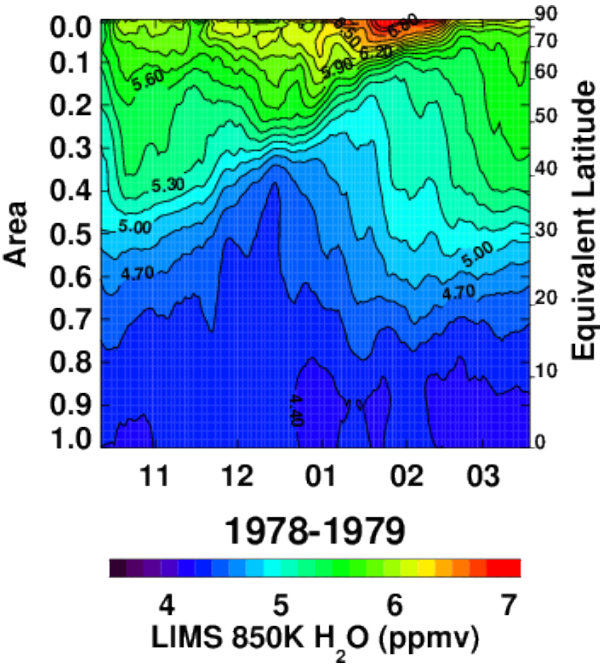


893

894 Figure 17—Area diagnostic plot of V6 Level 3 ozone for comparison with Figure 16. Ozone
895 contour interval is 0.2 ppmv. Tick marks on the abscissa indicate the 15th of each month.

896

897



898

899 Figure 18—As in Fig. 17, but for V6 H₂O at 850 K; contour interval is 0.15 ppmv.

900